Water Research 293 (2026) 125438

Contents lists available at ScienceDirect

Water Research

journal homepage: www.elsevier.com/locate/watres

Responses of ecological stability in subtropical coastal phytoplankton communities to varying N:P ratios under present and future scenarios

Jichen Chen [a,c,d,1], Yonglong Xiong [a,c,d,1], Jingke Ge [a], Xin Zhao [a], Yuan Feng [a], Xu Li [a], Chi Song [a], Xiao Yang [a], Rui Zhang [a], Jin-Yu Terence Yang [a], Wuchang Zhang [b], Shengyao Sun [a,c,d], Chao Zhang [e], Huijie Xue [a], Dazhi Wang [a], Kunshan Gao [a], Guang Gao [a,c,d,*]

[a] State Key Laboratory of Marine Environmental Science, College of Ocean and Earth Sciences, Xiamen University, Xiamen 361005, China
[b] CAS Key Laboratory of Marine Ecology and Environmental Sciences, Institute of Oceanology, Chinese Academy of Sciences, Qingdao, China
[c] Dongshan Swire Marine Station (D-SMART), Xiamen University, Dongshan, China
[d] National Observation and Research Station for the Taiwan Strait Marine Ecosystem, Xiamen University, Zhangzhou, China
[e] Institute of Environmental Research, Shandong University, Qingdao, 266237, China

HIGHLIGHTS

- Elevated N:P promotes phytoplankton blooms especially under the future scenario.
- Nitrogen restructuring can push phytoplankton biomass back to relative healthy level.
- Nitrogen restoration causes a shift from diatoms to dinoflagellates and chlorophytes.
- Climate change reduces the resistance and recovery capacity of coastal ecosystem.

GRAPHICAL ABSTRACT

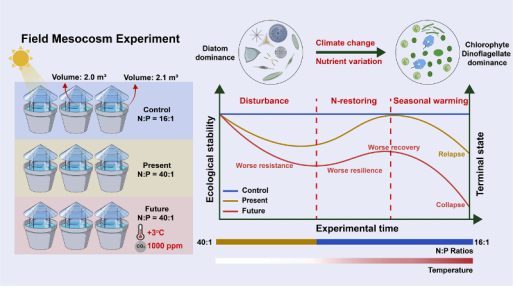

ARTICLE INFO

Keywords:
Climate change
Elemental stoichiometry
Ecological stability
Nutrient unbalance
Phytoplankton
Primary productivity

ABSTRACT

Anthropogenic activities are driving elevated N:P ratios in coastal waters and climate change. However, the ecological stability of plankton ecosystems under these combined stressors remains poorly understood. Using 32-day mesocosm experiments, we evaluated how subtropical plankton ecosystems respond to elevated N:P ratios (40:1) under present (20°C, 440 ppm CO_2) and future (23°C, 1000 ppm CO_2) scenarios in the first half period, followed by the next half period of restoration to Redfield ratio (16:1). A control group maintained a N:P ratio of 16:1 throughout the experiment. Elevated N:P stimulated phytoplankton biomass and primary productivity, with more pronounced effects observed under the future climate scenario. After 5-day nutrient restructuring, phytoplankton biomass and primary productivity returned to the control levels. However, a rapid rebound was detected after day 23, particularly under the future scenario. Relative to the present scenario, ecological stability (resistance, resilience, and recovery) of phytoplankton biomass and primary productivity declined in the future scenario. Furthermore, nutrient restructuring led to a marked shift from diatom- to dinoflagellate and chlorophyte-dominated assemblages, which was more significant in the future scenario. Elevated N:P ratios also enhanced grazing rates of zooplankton, with stronger effects in the future scenario, though grazing rates returned

* Corresponding author.
E-mail address: guang.gao@xmu.edu.cn (G. Gao).
[1] These authors contributed equally to this work.

https://doi.org/10.1016/j.watres.2026.125438
Received 18 September 2025; Received in revised form 28 December 2025; Accepted 21 January 2026
Available online 21 January 2026

to control levels following nutrient restoration. Elevated N:P did not affect elemental stoichiometry immediately but enhanced POC:POP and PON:POP by the end of the experiment, particularly in the future scenario. Our findings highlight that mitigating nitrogen inputs alone may be insufficient to restore coastal ecosystems; climate change would increase the challenges of coastal restoration due to nutrient restructuring.

1. Introduction

Coastal seas sustain the highest levels of marine primary productivity on Earth and underpin fisheries that feed hundreds of millions of people (Chavez et al. 2011, Dai et al. 2023a). These waters are bordered by landmasses that host >50% of the global population and generate ~50% of the world's GDP, especially across rapidly developing Asian economies (Dai et al. 2023a). Yet this socio-ecological prosperity is increasingly jeopardized by anthropogenic alteration of nutrient stoichiometry. Over the last five decades, global synthetic-fertilizer application has tripled, driving a 43% increase in riverine nitrogen (N) export and pushing the average N:P ratio in Chinese coastal waters from the canonical Redfield value of 16:1 to > in excess of 30:1 (Dai et al. 2023a). Such extreme N:P enrichment intensifies harmful algal blooms and systematically reshapes phytoplankton community structure (Dai et al. 2023b, Wang et al. 2021). Meta-analyses reveal a shift of phytoplankton community from diatoms to dinoflagellates as N:P rises (Wei et al. 2024, Xiao et al. 2018).

Empirical evidence from lakes and coastal ecosystems demonstrates that reducing external nitrogen can effectively suppress harmful algal blooms such as the near-full recovery of chlorophyll *a* and nitrogen-phosphorus content (Jeppesen et al. 2007, McCrackin et al. 2016). However, recovery patterns were influenced by the initial eutrophic conditions, with more eutrophic lagoons requiring longer recovery times and experiencing temporary setbacks during the process. These findings emphasize the importance of nutrient management and the complexity of plankton restoration, particularly in highly impacted ecosystems (Derolez et al. 2019). Meanwhile, nutrient-reduction programs have not universally achieved desired ecological outcomes, such as the complex and non-linear responses to subsequent nutrient abatement and failing to return to reference states (Duarte et al. 2008). The authors attributed this inertia to cumulative environmental changes that accumulated during the 30-year interval between eutrophication onset and management intervention, altering ecosystem dynamics and shifting baselines. These findings highlight the critical need to understand planktonic responses not only to nutrient perturbations but also to concurrent environmental change.

In parallel to nutrient stress, ocean warming and acidification are reshaping ecosystem structure and coastal primary production with complex effects, depending on species-specific thermal/acidification optima and co-limiting factors (Gao et al. 2020, 2021). Acidification can impede the diatom-to-dinoflagellate succession while enhancing viral and bacterial abundances (Huang et al. 2021). Long-term records combined with models indicate a poleward shift of the plankton species' distributions accompanied by increases in picoplanktonic cyanobacteria and small eukaryotes at the expense of large diatoms (Benedetti et al. 2021, MorÁN et al. 2010). These compositional changes manifest as systematic reductions in community mean cell diameter and a skewing of the biomass spectrum toward smaller size classes, consistent with the temperature–size rule predicted by metabolic theory.

Stability theory, with its mathematical foundations in differential equations and dynamical systems, broadly elucidates ecological system responses to perturbation (Ives and Carpenter 2007, McCann 2000). Stability theory provides a useful framework for evaluating the efficacy of restoration. Resistance (the capacity to withstand disturbance), resilience (the rate of recovery) and recovery (the degree of return to pre-disturbance conditions) are key metrics of ecological stability (Hillebrand et al. 2017). Thus, investigating how elevated N:P and subsequent nutrient reductions affect the resistance, resilience, and recovery of phytoplankton communities is of great significance for predicting the success of coastal restoration projects in a changing climate. Yet how elevated N:P and subsequent nutrient reductions modulate these stability properties of phytoplankton communities remains poorly resolved, particularly under the scenarios of climate change.

Whether phytoplankton communities—the energetic base of coastal food webs—will respond predictably to concurrent shifts in nutrient stoichiometry, temperature and CO_2, and whether nutrient management can still achieve desired ecological outcomes in the context of climate change, represents a critical knowledge gap. Here, we conducted a 32-day mesocosm experiment in subtropical coastal waters (Dongshan Bay, China) to test the hypothesis: Future warming (+3°C) and acidification (+560 ppm CO_2) will amplify biomass responses yet weaken stability metrics, making restoration more difficult. We integrated high-frequency measurements of chlorophyll *a*, primary productivity, plankton community structure, bacterial abundance, grazing rates and particulate organic stoichiometry. Our findings provide mechanistic insight into the efficacy of nitrogen management under ongoing global change and inform adaptive strategies for sustaining coastal ecosystem services.

2. Materials and methods

2.1. Mesocosms setup and experimental design

The mesocosm experiment was conducted from March 29 to April 30 in 2024 (32 days), at the Dongshan Swire Marine Station platform (D-SMART) of Xiamen University, Fujian Province, China (23.66°N, 117.49°E). The mesocosm system comprised nine thermoplastic polyurethane (TPU) bags (1.4 m in diameter, 1.3 m in height, and 2.0 m^3 in volume). To control temperature, each bag was placed in a white polyethylene (PE) tank (1.78, 2.2, and 1.3 m in bottom, top diameters, and depth, respectively) filled with freshwater (2.1 m^3) with a stainless-steel shelf to secure each TPU bag (Fig. S1). The mesocosms were deployed outdoors and exposed to natural sunlight to simulate ambient environmental conditions (Fig. S1). Nearshore seawater of D-SMART, filtered by 2 mm mesh to remove large organisms, was pumped to fill 9 bags simultaneously within 6 h. The nine mesocosms were assigned to three groups, each with three biological replicates. The three groups were control (N:P = 16:1, 20°C, and ambient CO_2 concentration of 440 ppm), elevated N:P (HN-P) in the present scenario (N:P = 40:1, 20°C, and ambient CO_2 concentration of 440 ppm) and elevated N:P (HN-F) in the future scenario (N:P = 40:1, 23°C, and CO_2 concentration of 1000 ppm). The N:P in control (Ctrl) represents an environment that is little affected by human activities (Redfield ratio) while the elevated N:P represents the scenarios in Chinese coastal waters due mainly to massive use of nutrient-rich synthetic fertilizers and their runoff into waterways (Dai et al. 2023a). The increased temperature and CO_2 levels correspond to the projected climate scenario by 2100 (IPCC 2023).

Initial concentrations of DIN (nitrate) and DIP (phosphate) were set as 12.8 and 0.8 μM for control and 32 and 0.8 μM for HN-P and HN-F treatments. To maintain nutrient availability and their ratios, nitrate and phosphate were supplemented daily during days 0–15 of the experiment, with their molar ratios of 16:1 control and 40:1 for HN-P and HN-F treatments. The concentrations of phosphate in seawater were measured every day. The added amounts of P were based on the consumed amounts and the volume of seawater, aiming to achieve the initial setting concentrations. The added amounts of N were based on the

ratio of 16:1 and 40:1 because N concentrations could not be measured at D-SMART. On day 16, the daily nutrient addition of N:P molar ratio was adjusted to 16:1 for all mesocosms to restructure nitrogen and phosphorus discharge to Redfield ratio. A total of 514.55 L of seawater was removed from each mesocosm bag of three groups for analytical assays. When the cumulative sampling volume approached 10% of the total culture volume (2,000 L), the system was replenished with filtered (through 0.1 μm) natural seawater that contained the corresponding set of nutrients for each treatment. Temperature was controlled by outer freshwater circulating via coolers (TY-10C-W; Sky One, China). To simulate the natural seasonal warming trend of coastal seawater, the temperature of all bags was increased by 1°C on days 15, 18, and 24, respectively. This adjustment resulted in final temperatures of 23°C for the control and HN-P groups, and 27°C for the HN-F group. CO_2 concentrations were maintained by aerating either ambient air or CO_2-enriched air, using CO_2 enrichers (CE100-D; Ruihua, China) for the latter.

2.2. Measurements of environmental parameters

The Photosynthetically Active Radiation (PAR) was measured using a real-time monitoring equipment (EKO, Japan), recorded per minute on the roof of D-SMART (Fig. S2A). Temperature was measured twice a day (5:30 and 14:30) using electronic thermometers (Deli8897, Deli, China). The pH was measured at 7:30 via a calibrated pH meter (Orion STAR A211, Thermo Scientific, USA), and total alkalinity (TA) was calculated by titrations. TA of seawater samples was determined via a multi-step titration procedure. Prior to analysis, seawater samples were filtered through a 0.45 μm cellulose acetate membrane and stored at 4°C until measurement, at which point they were equilibrated to room temperature (25°C). The HCl titrant (~0.006 mol L^{-1}) was standardized against 0.01 mol L^{-1} anhydrous sodium carbonate standard using methyl red-methylene blue mixed indicator. For each titration, an aliquot of 5 mL of sample was titrated with approximately 2 mL of standardized HCl to achieve a final pH between 3.5 and 3.9. TA was then calculated based on the respective volumes of the sample and acid, the measured pH value, and the corresponding hydrogen ion activity and activity coefficient. The other parameters, such as CO_2 concentration, were calculated via CO2SYS software based on the pH and TA value (Pierrot et al. 2011), using the equilibrium constants of K1 and K2 for carbonic acid dissociation (Roy et al. 1993).

2.3. Nutrient concentration measurement

Seawater samples were collected at 07:30 a.m. daily and immediately filtered through a cellulose acetate filter membrane (pore size: 0.45 μm) to remove particulate matter. Subsequently, 45 mL of the obtained filtrate was aliquoted into three equal 15-mL portions, which were separately transferred to high-density polyethylene (HDPE) centrifuge tubes and subjected to targeted preservation conditions based on the specific nutrient parameters to be analyzed. Specifically, the first portion was immediately frozen at −20°C for the subsequent determination of nitrate, nitrite, and phosphate concentrations, while the second portion was supplemented with chloroform (1‰, v/v) to inhibit microbial activity and prevent ammonium transformation before being stored at −20°C for ammonium concentration analysis, and the third portion was kept at 4°C to avoid potential degradation of silicate species, with the determination of dissolved silicate concentration completed within one week. The concentrations of nitrate, nitrite, ammonium, phosphate, and dissolved silicate were analyzed using an auto-analyzer (Model AA500, Seal Analytical Germany) under room temperature conditions. The limits of detection (LOD) were as follows: nitrate, 100 nM; nitrite, 40 nM; phosphate, 80 nM; ammonium, 30 nM; dissolved silicate, 200 nM.

2.4. Particulate organic carbon, nitrogen and phosphorus measurement and ratio

Seawater samples (50–600 mL) were collected at 08:00 on day 0, 15, 23, and 31, followed by filtering onto pre-combusted GF/F membrane, then stored at −20°C until subsequent analysis. For the determination of particulate organic carbon (POC) and particulate organic nitrogen (PON), the frozen GF/F filters were fumed with 35% (v/v) hydrochloric acid for 24 h and then dried at 60°C prior to analysis. Then POC and PON contents were measured via elemental analyzer (Vario EL Cube, Elementar, Germany). For the determination of particulate organic phosphorus (POP), the filtered GF/F filters were transferred to pretreated glass vials, followed by the addition of 2 mL of 0.017 M magnesium sulfate solution, and then dried at 95°C for 5 h. Subsequently, the glass vials were calcined at 450°C for 2 h, cooled to room temperature, and then 5 mL of 0.2 M HCl was added to each vial. The mixture was heated in a water bath at 80°C for 30 min and then cooled to room temperature. Finally, the samples were analyzed for POP content using an auto-analyzer (AA5, Seal Analytical, Germany), by the method described by Solórzano and Sharp (1980).

2.5. Chlorophyll a measurement

Seawater samples (25–1000 mL) were collected daily at 08:00 and filtered through GF/F membranes. The filtered membranes were transferred to centrifuge tubes, immersed in 100% methanol, and heated in an 80°C water bath for 6 minutes. Subsequently, the extracts were centrifuged at 8000 × *g* and 4°C for 10 minutes, and 2 mL of the supernatant was aliquoted for absorbance measurements. Absorbance was determined at wavelengths of 480, 510, 632, 652, 665, and 750 nm using a UV-visible spectrophotometer (UV1800, SHIMADZU, Japan). The absorbance values were calculated following Ritchie (2006).

2.6. Bacterial abundance measurement

Seawater samples were collected at 08:00 and filtered through GF/F membranes. Subsequently, 1.98 mL of the filtrate was mixed with 25% (v/v) glutaraldehyde which adjusted to the final concentration of glutaraldehyde 0.1% (v/v) for bacterial cell fixation. The mixture was vigorously vortexed, then incubated in the dark at room temperature for 30 mins. Then, the samples were frozen in liquid nitrogen and stored at −80°C until subsequent analysis. Prior to measurement, the cryopreserved samples were slowly thawed in a 37°C water bath. Following thawing, SYBR Green I was added to the samples to a final concentration of 1× , then incubated in the dark for 15 mins to ensure sufficient staining. Finally, the prepared samples were analyzed and calculated using a flow cytometer (CytoFLEX, Beckman, USA).

2.7. Carbon fixation measurement

Carbon fixation measurements were conducted every 2 days. For each measurement, 30 mL of seawater samples were aliquoted and spiked with 2.5 μCi $NaH^{14}CO_3$, followed by transfer to quartz tubes. Then the quartz tubes were incubated under corresponding temperature-controlled conditions prior to sunrise. After full-spectrum solar radiation exposure for the entire daytime, the water samples were filtered onto GF/F membranes to collect ^{14}C-labeled phytoplankton cells and then stored at −20°C until subsequent analysis. Prior to analysis, inorganic ^{14}C of frozen membranes was eliminated by acid fumigation and drying. Then, 5 mL of scintillation cocktail (Hisafe3, PerkinElmer, USA) was used to equilibrate the membranes, followed by measuring the radioactivity of the samples (LSC; Model LS 6500, Beckman Coulter, Brea, USA). Carbon fixation rates over 12 h and 24 h were calculated according to the method described by (Gao et al. 2017) with rates normalized to two units: per liter of water and per unit Chl *a* concentration. The 12 h and 24 h carbon fixation rates corresponded to

daytime primary productivity (DPP) and daily net primary productivity (NPP), respectively. Assimilation number was obtained by dividing primary productivity with Chl *a* concentration.

2.8. Community structure of phytoplankton measurement

For identification of microplankton (20–200 μm), seawater samples (1 L) were collected, fixed with acidic Lugol's iodine. Samples were stored in darkness at ambient temperature. After 24 h of static sedimentation, the supernatant was siphoned off to achieve a 10-fold concentration (100 mL). An aliquot of the concentrated sample was injected into a FlowCAM VS-4 equipped with a 10× objective and a 100 μm flow cell. Images were acquired at a flow rate of 0.2 mL min^{-1} and an imaging efficiency of 19.9%. Raw images of plankton, detritus and abiotic particles were automatically segmented and combined into contiguous full-frame mosaics for downstream processing.

For identification of mesoplankton (200 μm–2 mm), seawater samples (50 L) were gently passed through a 200 μm mesh plankton net. The retained organisms were resuspended, fixed with acidic Lugol's iodine and buffered formaldehyde (final concentration 1% v/v), and stored in darkness at room temperature. Subsamples were settled in Utermöhl chambers over 24 h and enumerated at either 200× or 400× magnification using an inverted microscope (Utermöhl 1958).

For data processing, individual organisms were isolated from background particles by cascading the Canny edge-detection and adaptive local-thresholding algorithms to generate single-region-of-interest (ROI) image stacks. Unambiguous images were enumerated directly; Ambiguous images were assigned to taxonomic categories using morphological and biological criteria. All ROIs were normalized to 128 × 128 pixels by centered cropping and background filling while preserving aspect ratio. Normalized images were then used to train a convolutional neural network (CNN)-based classifier, ensuring that neither geometric distortion nor background artefacts affected feature extraction.

For classification, denoising diffusion probabilistic model-Convolutional neural network was applied for the fine-grained classification of marine plankton. Based on above processes (Xue 2024), the abundance of phytoplankton was measured and the proportion of each category was calculated.

2.9. Grazing rate and zooplankton community structure measurement

Grazing rate was determined every four days by the dilution technique (Landry and Hassett 1982) (Table S1). From each mesocosm bag, unfiltered seawater was collected and combined with the same filtered (0.22 μm) seawater to obtain the dilution series of 100%, 75%, 50% and 25% whole seawater in acid-washed 1 L polycarbonate bottles. The bottles were incubated *in situ* alongside the bags with constant temperature-controlled water bath (12:00 h, local noon). After 24 h, the entire seawater was filtered onto GF/F membrane. Chlorophyll *a* (Chl *a*) concentrations in each dilution were quantified fluorometrically as described above.

Ciliate identification and enumeration followed the protocol detailed in section 2.8. For the copepod *Harpacticus uniremis* and cirripede larvae, 1 L samples were settled in 24 h for two times to obtain concentrated 5–11 mL samples. The concentrate was scanned and calculated to obtain absolute abundances (n) by the following method Utermöhl (1958). Representative images of each taxon were acquired using the Olympus cellSens Standard 1.17 imaging system interfaced with the microscope.

2.10. Resistance, resilience, recovery, and temporal stability estimates

Ecological stability was quantified through two complementary dimensions—functional stability (indexed by Chl *a* concentration and carbon fixation) and compositional stability (indexed by the abundances of phytoplankton and zooplankton species). Four stability parameters—resistance, resilience, recovery and temporal stability—were calculated following the conceptual and methodological frameworks (Hillebrand et al. 2017, Soulié et al. 2022).

Briefly, daily log-response ratios (LRR) were computed for the HN-P and HN-F treatments relative to the Ctrl. Resistance was defined as the mean LRR over the disturbance period (days 1–15); it quantifies the capacity of the community to withstand nutrient perturbation. Resilience was estimated by the slope of a linear regression of LRR against time during the restoration interval (days 16–20 or days 16–31), reflecting the instantaneous rate of recovery following nutrient re-equilibration. Recovery was expressed as the LRR value on the last day of each restoration period (days 20 and 31), indicating the degree to which the treated communities converged on the control. Temporal stability was calculated as the inverse of the standard deviation of resilience, providing a measure of variability in the recovery trajectory. All formulas and their ecological interpretations are summarized in Table S2.

2.11. Statistical analysis

To mitigate the effects of noise and irregularities in the continuous time-series data, a smoothing procedure was implemented using generalized additive mixed models (GAMM). The analysis encompassed key variables, including environmental parameters, Chl *a* concentration, total bacterial abundance, primary productivity and assimilation number, abundance and proportion of phytoplankton, grazing rates and zooplankton abundance. Values of POC, PON, and POP contents and their ratios are reported as the mean ± standard deviation of three independent biological replicates. Statistical analyses were performed in SPSS 25.0. Repeated-measures (RM) ANOVA was employed to assess the interactive effects of time and treatment on the response variables. Daily differences among treatments were evaluated by one-way (OW) ANOVA followed by Fisher's LSD post-hoc test; significance was accepted at $p < 0.05$ when Levene's test was satisfied, or at $p < 0.01$ when it was not. Differences in stability parameters between treatments were examined using independent-samples t-tests, with significance set at $p < 0.05$. All figures were generated with Origin 8.5.

3. Result

3.1. Variations in key environmental parameters

Nutrient dynamics throughout the cultivation period are shown in Fig. 1. Time had significant interactive effects with treatment on the nitrogen (N), phosphorus (P), silicon (Si) concentrations, and the DIN: DIP ratio (Table S3). NO_x^- (nitrate + nitrite) and DIN concentrations under HN-F and HN-P peaked in the middle of the cultivation period and then decreased, whereas those under Ctrl remained relatively stable (Fig. 1A, C). NO_x^- and DIN concentrations in HN-F and HN-P were significantly higher than in Ctrl throughout the period (Table S4). The NH_4^+ concentrations fluctuated from 0 to 9.81 μM with no differences among three groups at most timepoints (Fig. 1B). The PO_4^{3-} concentrations decreased to nearly zero within the first eight days and then fluctuated between 0.02 and 0.97 μM, with no differences among three groups at most timepoints (Fig. 1D). DSi concentrations showed a decreasing trend during the first 13 days, with the decreasing rate following the order: HN-F > HN-P > Ctrl (Fig. 1E). Afterwards, they remained very low till the end. The DIN: DIP ratio under Ctrl kept lower values (1.71–24.33) in the whole period while under HN-P and HN-F, the ratio showed a trend of first rising and then decreasing, ranging from 22.63 to 975.52 (Fig. 1F). Temperature and CO_2 levels under HN-F

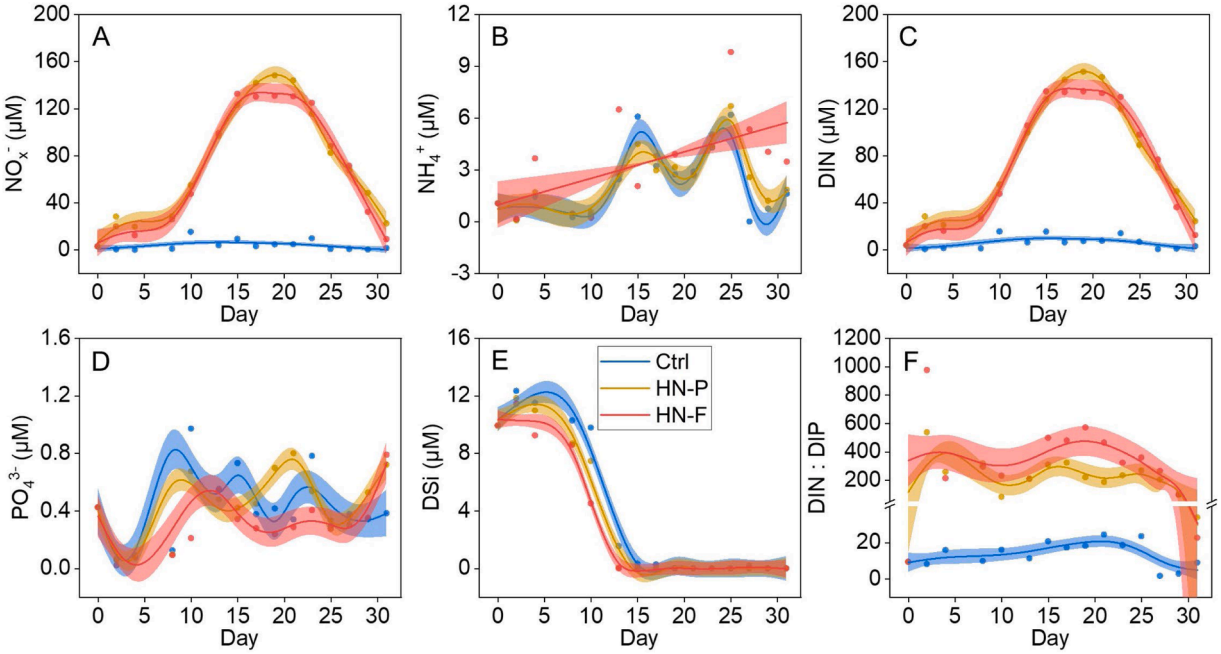

Fig. 1. Nutrient levels under different treatments. Nitrate and nitrite, NO_x^- (A), ammonium, NH_4^+ (B), dissolved inorganic nitrogen, DIN (C), phosphate, PO_4^{3-} (D), dissolved silicate concentration, DSi (E), and DIN:DIP ratio (F). Note: Ctrl, HN-P, and HN-F represent control, high N:P ratio in the present scenario, and high N:P ratio in the future scenario, respectively. Each dot represents one of n = 3 biological replicates and shaded areas denote 95% confidence intervals.

were higher than those under HN-P and Ctrl while salinity levels in three groups were similar throughout the experiment (Fig. S2&S3).

3.2. Accumulation of particulate organic carbon, nitrogen and phosphorus

Variations in particulate organic carbon (POC), nitrogen (PON), phosphorus (POP), and their ratios are presented in Fig. 2. Time had significant interactive effects with treatment on POC and PON contents (Table S3). POC, PON, and POP contents increased over time, with the magnitude of increase following: HN-F > HN-P > Ctrl (Fig. 2A-C). Thus, at most time points, POC, PON, and POP contents followed the order: HN-F > HN-P > Ctrl, although differences were statistically insignificant at several points (Table S4).

Time had significant interactive effect with treatment on the POC:PON ratio (Fig. 2D; Table S3). The POC:PON ratio in all treatments first decreased and then increased which was most evident under Ctrl. POC:PON ratio in Ctrl was significantly higher than in HN-P and HN-F in the end. Time had significant effect on the POC:POP ratio (Fig. 2E; Table S3), which also first decreased then increased in all groups. By the end period, the POC:POP ratio was highest in HN-F, though differences among groups were insignificant. For the PON:POP ratio, time had a

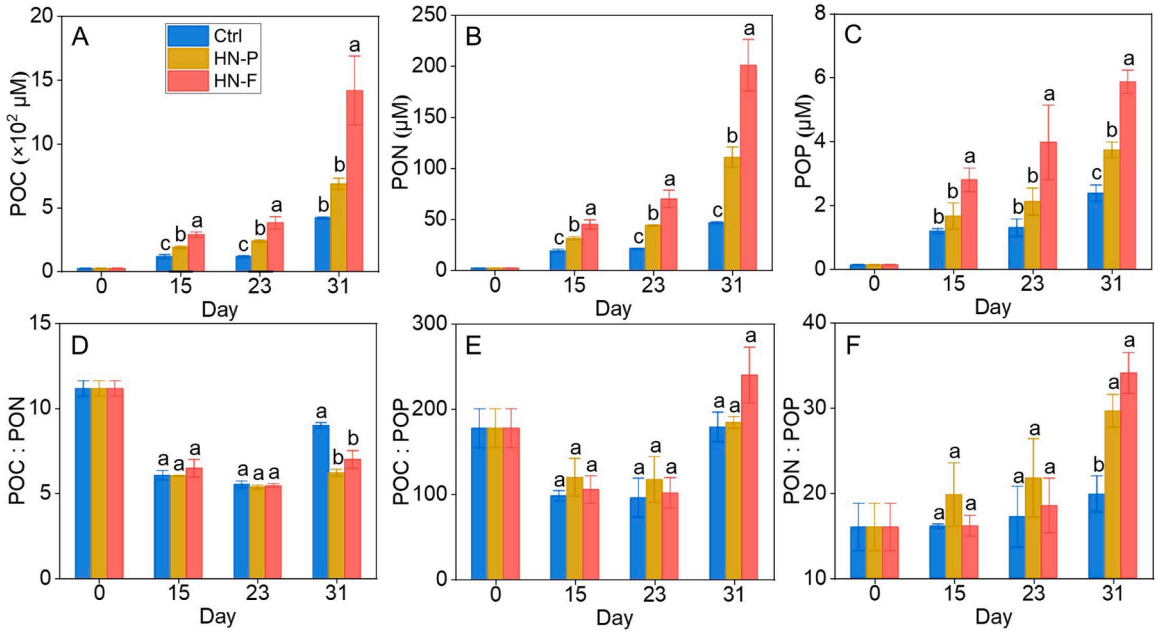

Fig. 2. Particulate organic matter in seawater under different treatments. POC (A), PON (B), POP (C), POC:PON ratio (D), POC:POP ratio (E), PON:POP ratio (F). Different letters represent the significant difference between groups at each time point ($p < 0.05$). Note as Fig. 1.

significant interactive effect with treatment (Fig. 2F; Table S3). The PON:POP ratio increased over time in all treatments, with HN-F showing the largest increase by the end. HN-P and HN-F significantly enhanced the PON:POP ratio compared to Ctrl on day 31 (Table S4).

3.3. Changes in Chl *a* concentration and total bacterial abundance

Temporal variations in Chl *a* concentration and bacterial abundance are shown in Fig. 3. Time had a significant interactive effect with treatment on Chl *a* concentration (Table S3). Chl *a* concentration in Ctrl increased slowly throughout the culture period, while that in HN-P and HN-F fluctuated during the first 23 days before rising rapidly (Fig. 3A). Specifically, Chl *a* concentration in HN-P and HN-F increased then decreased between days 10–20. HN-P had higher Chl *a* concentration than Ctrl between days 2–10, 13–19, and 21–31, while HN-F showed higher Chl *a* concentration than Ctrl throughout the period. From day 8 onward, HN-F had higher Chl *a* concentration than HN-P, with HN-F reaching over 2-fold and 6-fold higher values than HN-P and Ctrl, respectively, by the end.

Time had a significant interactive effect with treatment on total bacterial abundance (Table S3). After day 6, total bacterial abundance showed rising trends, which were particularly evident for HN groups (Fig. 3B). HN-P had significantly higher bacterial abundance than Ctrl on days 13, 15, 21, 23, and 31, while HN-F was markedly higher than Ctrl between days 21–27 (Table S4). On day 10, HN-F had significantly higher bacterial abundance than HN-P (Table S4).

3.4. Variation of carbon fixation in daytime and whole day

Time had a significant interactive effect with treatment on DPP, NPP, assimilation number$_D$ and assimilation number$_N$ (Table S3). DPP in all three groups remained relatively stable over the first 10 days, followed by varying degrees of oscillation, with HN-F showing the largest amplitude (Fig. 4A). HN-P had significantly higher DPP than Ctrl on days 6, 15, 17, and 23, while HN-F was significantly higher than Ctrl from day 13 onward. From day 8, HN-F had higher DPP than HN-P until the end (Table S4). NPP showed a similar trend to DPP (Fig. 4B). HN-P had significantly higher NPP than Ctrl between days 13–17, while HN-F was significantly higher than both HN-P and Ctrl on 80% of days from day 8 to the end (Table S4).

Assimilation number$_D$ in all treatments first increased and then decreased with strong oscillations (Fig. 4C). HN-P had significantly higher assimilation number$_D$ than Ctrl on days 4, 6, 10, and 13, whereas HN-F was significantly lower than Ctrl on days 10 and 17, and lower than HN-P on days 6, 10, and 13 (Table S4). Similar to assimilation number$_D$, the assimilation number$_N$ also first increased and then decreased with large fluctuations (Fig. 4D). HN-P had significantly higher assimilation number$_N$ than Ctrl on days 4, 6, 10, and 13, while HN-F was significantly higher than Ctrl on days 6, 10, and 29, and higher than HN-P on days 13 and 17 (Table S4).

3.5. Variation of phytoplankton groups and community structure

Time had significant interactive effects with treatment on the abundance and proportion of chlorophytes, diatoms, dinoflagellates, and cyanobacteria, except for dinoflagellate proportion, which was only affected by time (Table S3). Chlorophyte abundance increased slowly over days 0–17 in all treatments, then rose rapidly, with HN-F reaching the highest value by the end (Fig. 5A). HN-P had significantly higher chlorophyte abundance than Ctrl on days 5, 7, 19, and 21, while HN-F was significantly higher than Ctrl over days 15–29 and higher than HN-P over days 15–29 (except day 23; Table S4). The chlorophyte proportion in all treatments first increased, then decreased, and then increased again (Fig. 5B). HN-P had a significantly lower proportion than Ctrl on days 9, 15, and 17; HN-F was lower than Ctrl on days 9, 13, and 15 but higher on days 19 and 21, and lower than HN-P on day 9 but higher over days 17–21 (Table S4).

Diatom abundance exhibited a unimodal temporal pattern, characterized by an initial rapid increase followed by a subsequent decline (Fig. 5C). Among the treatments, HN-F displayed the earliest and sharpest ascent. Peak values in HN-P and Ctrl lagged behind HN-F, appearing sequentially. HN-P had significantly higher diatom abundance than Ctrl on days 7, 9, 15, and 17; HN-F was higher than Ctrl on days 9–17, 25, 29, and 31, and higher than HN-P on days 9–13, 17, 29, and 31 (Table S4). In parallel, the relative contribution of diatoms to total phytoplankton biomass followed a trimodal trajectory—initial decrease, subsequent rebound, and final reduction (Fig. 5D). HN-P had a significantly higher proportion than Ctrl on days 9, 15, and 17; HN-F was higher than Ctrl on days 9–13 and higher than HN-P on days 9 and 11 (Table S4).

Dinoflagellate abundance exhibited a monotonic increase throughout the observation period, punctuated by a transient dip on day 19 (Fig. 5E). HN-P was higher than Ctrl over days 7–9; HN-F was higher than Ctrl on days 7–13, 27, and 29, and higher than HN-P on days 9–15 and 29 (Table S4). The temporal dynamics of dinoflagellate proportion diverged among treatments. Ctrl displayed an abrupt initial rise followed by a sharp decline; HN-P manifested a moderate increase and a subsequent decrease; HN-F showed only a marginal increase before decreasing (Fig. 5F). Statistically, HN-P was lower than Ctrl on days 7 and 9, but significantly higher on days 15 and 17. HN-F exceeded Ctrl on days 7 and 9, yet became markedly lower on days 13–19, 23, and 31. Relative to HN-P, HN-F was higher on day 7 but significantly lower on day 31 (Table S4).

Cyanobacterial abundance followed a unimodal trajectory, characterized by a progressive rise followed by a pronounced decline. Peak abundance was recorded on day 17 in both HN-F and HN-P, whereas Ctrl

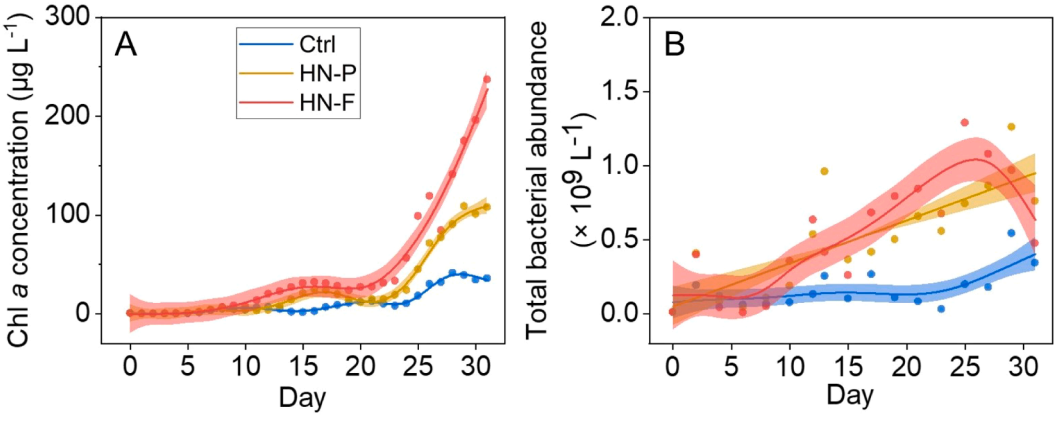

Fig. 3. Chl *a* concentration (A) and total bacterial abundance (B) in seawater under different mesocosm treatments. Note as Fig. 1.

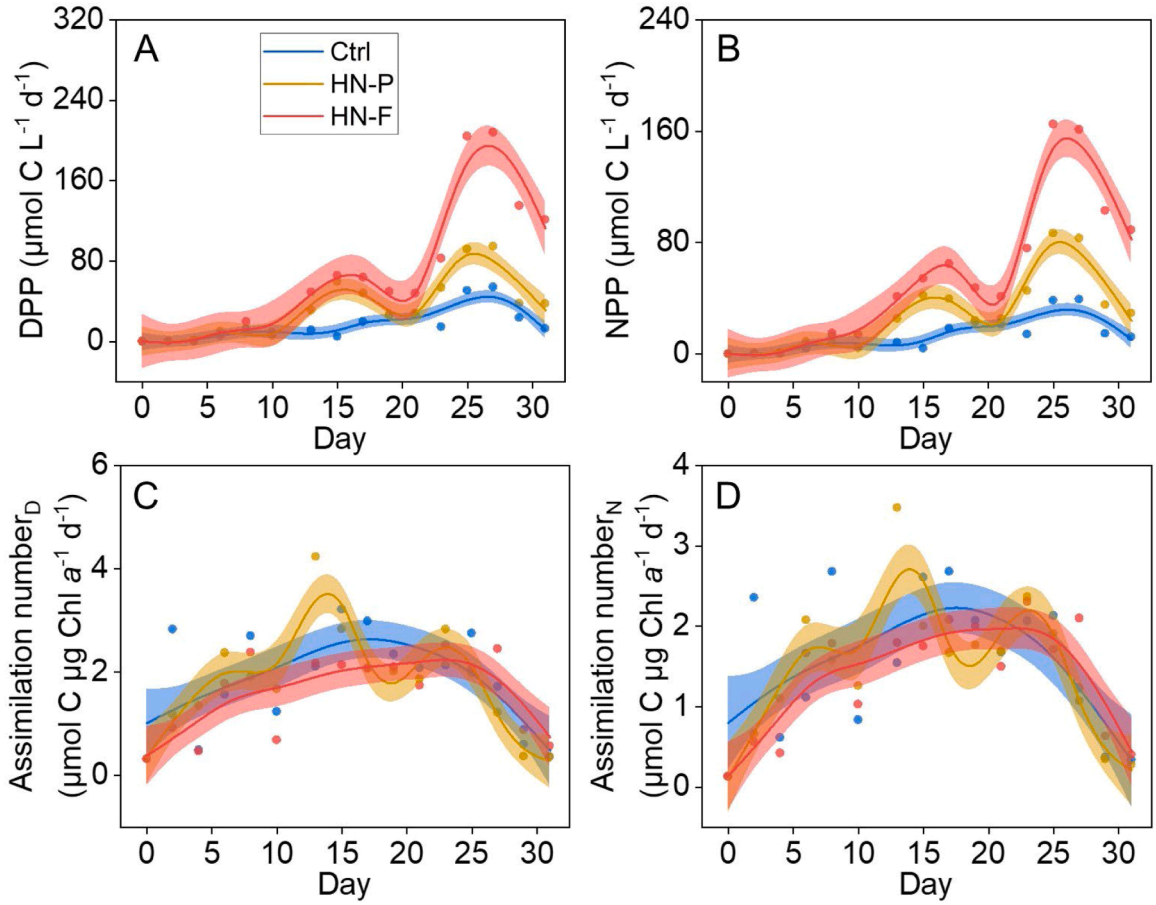

Fig. 4. Primary productivity and assimilation number of phytoplankton under different mesocosm treatments. Daytime primary productivity (12 h), DPP (A), net primary productivity (24 h), NPP (B), assimilation number based on DPP (Assimilation number$_D$) (C), and assimilation number based on NPP (Assimilation number$_N$) (D). Note as Fig. 1.

reached its maximum four days later, on day 21 (Fig. 5G). Relative to Ctrl, HN-P exhibited significantly lower abundance on days 13 and 21 (Table S4). In contrast, HN-F surpassed HN-P on days 15, 17, and 31. The proportional representation of cyanobacteria displayed a triphasic pattern: an initial sharp decrease, a mid-period fluctuation, and a terminal decline (Fig. 5H). Compared with Ctrl, HN-P exhibited a significantly lower proportion on days 13 and 21. HN-F was consistently lower than Ctrl on days 9, 13, and 21, yet transiently exceeded HN-P on day 15 (Table S4).

In the first half period, high N:P significantly increased the proportion of diatoms, making it the most dominant group by the end of nutrient disturbance (Fig. S4). Following restoration, a shift in dominance occurred, with chlorophytes progressively becoming the dominant taxa in the temporal sequence HN-F > HN-P > Ctrl. This suggests that Si-deficiency driven shift can be accelerated by ocean warming and acidification.

3.6. Variation of grazing rate and zooplankton community structure

Time had significant interactive effects with treatment on grazing rate, *Harpacticus uniremis* abundance, and ciliate abundance, while time alone significantly affected Cirripedia larva abundance (Table S3). Grazing rates fluctuated strongly, increasing from day 5 then decreasing from day 17 onward (Fig. 6A). On day 25, HN-P had a significantly lower grazing rate than Ctrl and HN-F. HN-F showed the highest grazing rate between days 9 and 21, while Ctrl was highest on days 25 and 29 (Table S4).

The identified zooplankton species were shown in Fig. S5. *Harpacticus uniremis* was not detected until day 23 (Fig. 6B). Subsequently, HN-F attained significantly higher abundance than Ctrl on day 31 and consistently exceeded HN-P on both days 23 and 31 (Table S4). Cirripedia larval abundance exhibited a unimodal trajectory, with an initial rise followed by a progressive decline (Fig. 6C). HN-P was significantly higher than Ctrl and HN-F on day 15, and the highest on days 15 and 23 (Table S4). Ciliate abundance increased monotonically throughout the experiment, with HN-F registering the steepest increment (Fig. 6D). HN-P surpassed Ctrl on days 7–11, 17, and 31, whereas HN-F exceeded Ctrl on days 7, 9, 15, 17, 27, and 31. Moreover, HN-F was significantly higher than HN-P on days 11–15 and 27 (Table S4).

3.7. Ecological stability

The first 15 days were defined as the disturbance period, with nutrient restructuring initiated on day 16. Days 16–20 and 16–31 were designated as recovery periods. Ecological stability (resistance, resilience, recovery, and temporal stability) for days 1–20 was analyzed based on Chl *a* concentration, carbon fixation, and phytoplankton/zooplankton abundance (Table 1).

The resistance of Chl *a* concentration was lower in HN-P (0.425) than in HN-F (0.884), indicating higher sensitivity to nitrogen enrichment in HN-F. The absolute resilience value of Chl *a* was higher in HN-P (-0.556) than in HN-F (-0.413), suggesting stronger resilience in HN-P. Chl *a* recovery was closer to 0 in HN-P (-0.028) than in HN-F (0.803), indicating recovery in HN-P but not in HN-F. For assimilation number$_D$ and assimilation number$_N$, resistance was positive in HN-P (over-performance) and negative in HN-F (under-performance), with greater

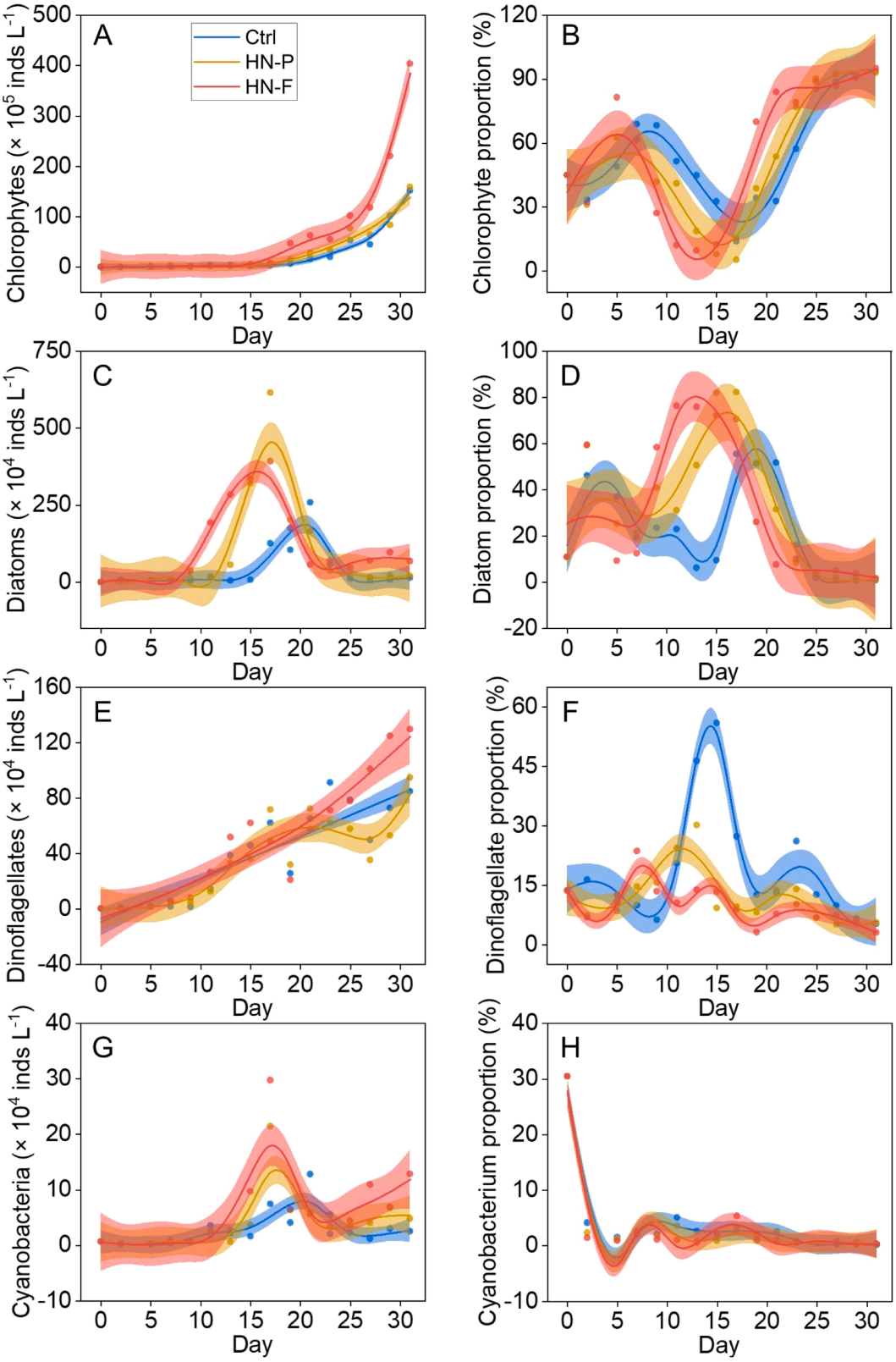

Fig. 5. Abundance and proportion of chlorophytes (A&B), diatoms (C&D), dinoflagellates (E&F), and cyanobacteria (G&H) under different mesocosm treatments. Note as Fig. 1; inds represents individuals.

deviation from 0 in HN-F, indicating higher sensitivity to elevated N:P in the future scenario. The resistance of phytoplankton and zooplankton abundance was closer to 0 in HN-P than in HN-F, indicating better resistance in HN-P. These results suggest that global warming combined with elevated CO_2 weakens plankton community resistance under nitrogen enrichment. Similar to Chl *a*, chlorophyte abundance showed higher resilience in HN-P (higher absolute resilience value) and faster recovery (recovery closer to 0) than in HN-F, though neither fully

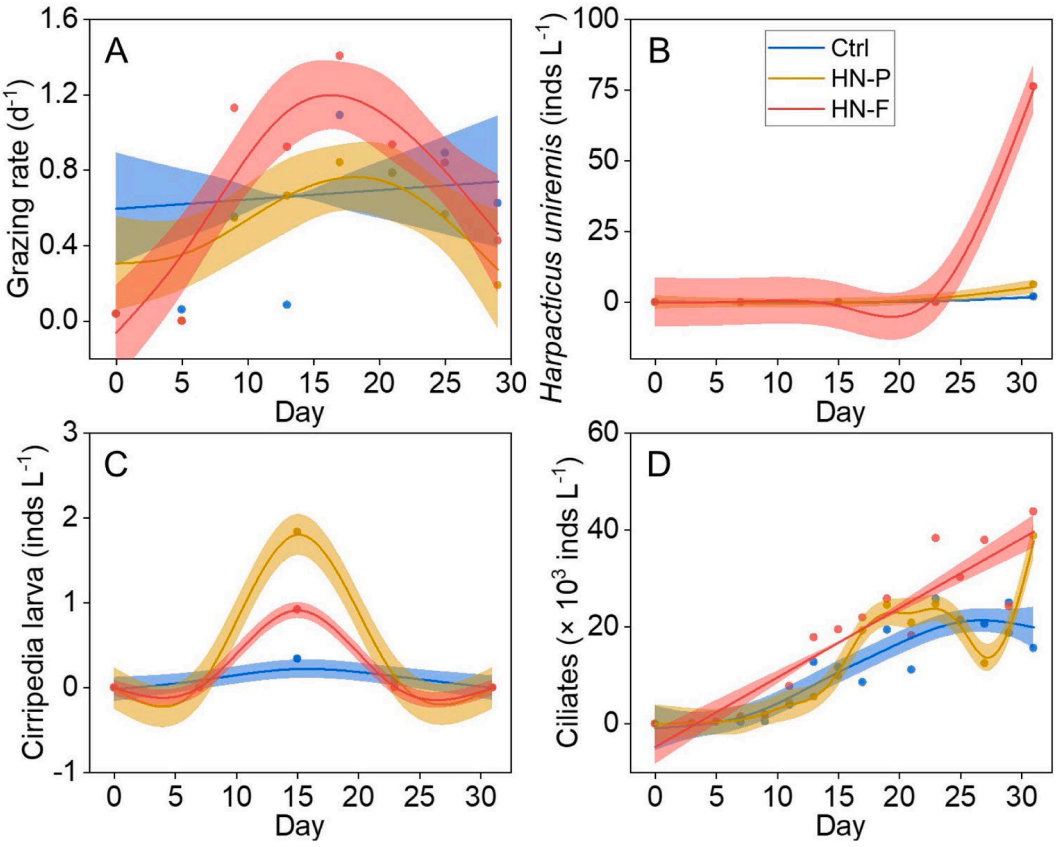

Fig. 6. Grazing rate (A), and abundance of *Harpacticus uniremis* (B), Cirripedia larva (C), and ciliates (D) under different mesocosm treatments. Note as Fig. 1; inds represents individuals.

recovered post-nutrient restructuring.

For the 31-day period, resistance values were identical to the 20-day period due to the same 15-day disturbance. By day 31, Chl *a* recovery was closer to 0 in HN-P than in HN-F, indicating stronger recovery capacity. HN-P also showed better recovery in DPP, NPP, and the abundance of chlorophytes, diatoms, and cyanobacteria (Table 1).

4. Discussion

4.1. Restoring phytoplankton biomass by reducing nitrogen input

Increased N:P stimulated phytoplankton growth and led to algal blooms in this study, corroborating the observation that progressive nitrogen enrichment is fueling larger and more frequent blooms in coastal waters worldwide (Dai et al. 2023a, Dai et al. 2023b). The occurrence of an algal bloom is defined as when the Chl *a* concentration in seawater exceeds 16 μg L^{-1} (Jiang and Zhang 2018). Re-adjusting the N:P supply to the canonical Redfield ratio (16:1) successfully restored Chl *a* to control levels by day 20, confirming that direct nitrogen input regulation can be an effective short-term restoration lever—analogous to successful nutrient-input reductions in freshwater lakes (Jeppesen et al. 2007). However, the Chl *a* concentration under the HN-P treatment rebounded rapidly after day 23, which may be related to the combination of higher DIN levels and the concurrent rise in seawater temperature (Fig. S2B & Fig. 1F). When compared to the control, the temperatures under HN-P and the control were the same, with the main difference being DIN level. When compared to the period of days 15–20, the driver should be rising temperature because the DIN levels during days 23–31 were even lower than those during days 15–20. In addition, when comparing HN-P and HN-F, HN-F had a higher Chl a concentration, while the main difference between these two treatments was temperature rather than DIN level. This aligns with findings by Feng et al. (2023) that moderate temperature increases promote algal bloom occurrence in Chinese coastal waters. These findings highlight the need to consider multiple environmental drivers when restoring phytoplankton biomass. Moreover, continuous nitrogen input resulted in the overloading of nitrogen in the enclosed experimental system, which could delay or prevent the effectiveness of nutrient restoration. The rising bacterial abundance in HN likely enhanced nitrogen recycling, which may have contributed to the post-restructuring rise in Chl *a* concentration despite nutrient regulation (Fig. 3B). In inner bays with limited water exchange, nitrogen pollution is recalcitrant to elimination, increasing ecosystem vulnerability. For example, algal blooms in Jakarta Bay predominantly occur during the dry season and transitional monsoon periods, characterized by weak turbulence, low current velocity, and stable nutrient conditions (Damar et al. 2021). Thus, while nitrogen restructuring can alleviate nitrogen overloading, water exchange remains a critical regulatory factor for enhancing restoration efficacy.

When increased N:P combined with warming and acidification, it resulted in higher phytoplankton biomass during the whole culture period. In addition to nitrogen and temperature, CO_2 is also an essential environmental factor that can affect growth of phytoplankton. Increased CO_2 can commonly stimulate carbon fixation and growth of microalgae because current CO_2 levels are limited for full operation of microalgal Rubisco (Raven et al. 2011). Notably, phytoplankton biomass (indexed by Chl *a*) in the future scenario exhibited lower resistance and resilience to elevated N:P compared to the present scenario. This indicates heightened sensitivity of phytoplankton assemblages to nitrogen enrichment and impaired recovery capacity under future climate conditions. Given the practical challenges of mitigating temperature and CO_2 levels in coastal waters, our findings underscore the urgency of

Table 1
Ecological stability parameters of phytoplankton communities exposed to varying N:P ratios and climate scenarios.

		Resistance (a)	Resilience (b)	Recovery (c)	Temporal stability (d)
20 days					
Chl *a*	HN-P	**0.425 ±0.039***	**-0.556 ±0.011***	**-0.028 ±0.001***	91.844
	HN-F	**0.884 ±0.064***	**-0.413 ±0.011***	**0.803 ±0.101***	94.465
DPP	HN-P	0.655 ±0.102	-5.659 ±0.689	0.001 ±0.360	1.451
	HN-F	0.679 ±0.041	-5.475 ±0.593	0.582 ±0.155	1.686
Assimilation $number_D$	HN-P	**0.102 ±0.110***	-5.720 ±0.505	-0.107 ±0.063	1.980
	HN-F	**-0.348 ±0.045***	-5.758 ±0.513	-0.187 ±0.139	1.950
NPP	HN-P	0.574 ±0.083	-5.681 ±0.630	0.106 ±0.356	1.586
	HN-F	0.733 ±0.036	-5.458 ±0.534	0.651 ±0.024	1.874
Assimilation $number_N$	HN-P	**0.013 ±0.051***	-5.737 ±0.452	0.004 ±0.104	2.213
	HN-F	**-0.301 ±0.105***	-5.736 ±0.457	-0.111 ±0.016	2.188
Chlorophytes	HN-P	**0.074 ±0.047***	**-5.609 ±0.472***	**0.523 ±0.203***	2.121
	HN-F	**0.404 ±0.034***	**-0.045 ±0.024***	**1.341 ±0.053***	41.503
Dinoflagellates	HN-P	**0.255 ±0.101***	-5.785 ±0.475	-0.032 ±0.561	2.106
	HN-F	**0.634 ±0.068***	-5.730 ±0.431	-0.139 ±0.166	2.318
Diatoms	HN-P	**1.204 ±0.159***	-5.826 ±0.988	-0.941 ±1.009	1.012
	HN-F	**1.730 ±0.078***	-5.729 ±0.907	-1.582 ±0.362	1.103
Cyanobacteria	HN-P	**-0.049 ±0.081***	-5.773 ±0.756	-0.892 ±0.468	1.322
	HN-F	**0.301 ±0.120***	-5.541 ±0.817	-0.833 ±0.063	1.224
Ciliates	HN-P	**0.178 ±0.076***	-5.481 ±0.533	0.603 ±0.200	1.877
	HN-F	**0.579 ±0.037***	-5.500 ±0.505	0.465 ±0.228	1.979
31 days					
Chl *a*	HN-P	**0.425 ±0.039***	-0.002 ±0.033	**1.072 ±0.250***	30.112
	HN-F	**0.884 ±0.064***	0.006 ±0.027	**1.859 ±0.253***	35.969
DPP	HN-P	0.655 ±0.102	**0.024 ±0.017***	**1.065 ±0.085***	60.192
	HN-F	0.679 ±0.041	**0.087 ±0.008***	**2.216 ±0.198***	130.231
Assimilation $number_D$	HN-P	**0.102 ±0.110***	-0.003 ±0.030	-0.003 ±0.165	33.509
	HN-F	**-0.348 ±0.045***	0.051 ±0.031	0.361 ±0.450	31.758
NPP	HN-P	0.574 ±0.083	0.039 ±0.021	**0.868 ±0.145***	47.287
	HN-F	0.733 ±0.036	0.078 ±0.009	**1.980 ±0.134***	115.872
Assimilation $number_N$	HN-P	**0.013 ±0.051***	0.010 ±0.019	-0.196 ±0.107	52.908
	HN-F	**-0.301 ±0.105***	0.041 ±0.017	0.130 ±0.330	57.504
Chlorophytes	HN-P	**0.074 ±0.047***	-0.045 ±0.027	**0.006 ±0.293***	36.481
	HN-F	**0.404 ±0.034***	-0.045 ±0.024	**0.926 ±0.341***	41.503
Dinoflagellates	HN-P	**0.255 ±0.101***	-0.019 ±0.030	0.104 ±0.129	32.896
	HN-F	**0.634 ±0.068***	0.056 ±0.034	0.410 ±0.179	29.619
Diatoms	HN-P	**1.204 ±0.159***	**-0.006 ±0.054***	**0.245 ±0.410***	18.613
	HN-F	**1.730 ±0.078***	**0.153 ±0.025***	**1.520 ±0.159***	39.977
Cyanobacteria	HN-P	**-0.049 ±0.081***	0.022 ±0.016	**0.616 ±0.266***	61.813
	HN-F	**0.301 ±0.120***	0.072 ±0.030	**1.610 ±0.205***	33.816
Ciliates	HN-P	**0.178 ±0.076***	-0.031 ±0.001	0.906 ±0.074	938.417
	HN-F	**0.579 ±0.037***	-0.008 ±0.031	1.000 ±0.250	32.635

Abbreviation: Bold numbers with * represent the significant difference between HN-P and HN-F ($p < 0.05$).

reducing CO_2 emissions, enhancing carbon sequestration, and mitigating climate change to preserve ecosystem stability.

4.2. *Restructuring N:P input changed the phytoplankton community structure*

Prior to nutrient restoration, continuous nitrogen enrichment triggered a surge of diatom abundance (72–82% proportion on day 15 in HN conditions), which was particularly pronounced for the future scenario. In contrast, the stimulative effects of nitrogen enrichment on other phytoplankton (chlorophytes, dinoflagellates and cyanobacteria) were not as significant as diatoms, suggesting that elevated N:P ratios could specifically drive diatom-dominated blooms. This finding aligns with the phenomenon observed in Jakarta Bay, where increased N:P ratios from 2010 to 2013 were linked to the occurrence of diatom-dominated phytoplankton blooms (Sidabutar et al. 2016).

After restructuring, the diatoms and cyanobacteria declined sharply over time while dinoflagellates and chlorophytes showed an increasing trend. The decreased diatom abundance may be mainly caused by DSi exhaustion, a well-documented phenomenon during algal blooms (Ryan et al. 2017, Sieracki et al. 1993). Moreover, the increase in diatom abundance prior to restoration promoted zooplankton growth, thereby intensifying grazing pressure, which in turn accelerated the subsequent decline in the diatom population. The shift from diatoms to dinoflagellates is consistent with field observations of algal bloom succession (Wei et al. 2024). The dying diatoms could supply enough food for the growth of dinoflagellates. When eutrophication combined with warming and acidification, dinoflagellate abundance was further improved, probably because dinoflagellates prefer high N:P ratios and warmer environments. The shift in phytoplankton succession from diatoms to dinoflagellates would transition amnesic shellfish poisoning (e.g., domoic acid) to paralytic shellfish poisoning (e.g., saxitoxin, gonyautoxin). In addition to dinoflagellates, another winner after restoration is chlorophytes, and the dominance of chlorophyte in phytoplankton community was further strengthened in the future scenario, which is related to increasing temperature. A previous study has predicted a gradual shift toward smaller primary producers in a warmer ocean (MorÁN et al. 2010). Our findings support their prediction since most chlorophytes are smaller than 2 μm in this study. In terms of cyanobacteria, another pico-phytoplankon group, their biomass under HN-F was also higher than that under HN-P and the control, suggesting that they could benefit from ocean warming and acidification. However, their proportion in the community decreased after nutrient restoration (Fig. 5H & Fig. S4). This phenomenon can be attributed to reduced competitive ability of cyanobacteria against chlorophytes. In Acton Lake, chlorophytes substantially exceeded cyanobacteria during spring

under P-limited condition (high N:P ratio), whereas a converse pattern was observed during summer under N-limited condition (low N:P ratio) (Atwood and Knoll 2025). In the hyper-eutrophic reservoir, chlorophyte abundance consistently exceeded that of cyanobacteria by nearly 2-folds at both the inflow and outflow sites (Andersen et al. 2019). Collectively, these results support the competitiveness of chlorophytes relative to cyanobacteria under high N:P or eutrophic conditions.

4.3. Plankton community structure changed the grazing rate

The grazing rates under HN had an increasing trend from days 5 to 17 and then decreased till the end of culture, consistent with the trend of diatom abundance rather than the other three phytoplankton taxa. This indicates that diatoms are the primary driver of secondary producer grazing. This could be attributed to two aspects. Firstly, diatom is the dominant taxa of phytoplankton during the first 17 days. Secondly, diatoms are palatable to a broad range of secondary producers, directly influencing grazing behavior (Zadereev et al. 2023). The temporal pattern of Cirripedia larva abundance, which mirrored diatom dynamics, further supports this conclusion.

Ciliate abundance showed a similar trend to chlorophyte abundance, suggesting that increased chlorophyte biomass may drive ciliate proliferation, as ciliates are known to graze on picophytoplankton such as chlorophytes (Cowlishaw 2002). It is worth noting that although Chl *a* concentration increased dramatically during the late stage of culture, the grazing rate did not increase but decreased. This could be attributed to increased chlorophyte proportion. As picophytoplankton, these chlorophytes are less accessible to zooplankton and other secondary producers compared to nano- and microphytoplankton (Pešťová et al. 2008). Moreover, a reduction in the grazing rate likely diminished the top-down control on the phytoplankton community, thereby promoting the accumulation of Chl *a*. Furthermore, HN-F enhanced the abundances of *Harpacticus uniremis* and ciliates particularly in the late stage of culture, indicating that future ocean conditions may promote zooplankton biomass through increased phytoplankton production.

4.4. Changed elemental stoichiometry

POC, PON, and POP contents in seawater increased over time, with particularly marked accumulation in the late stage, which is consistent with Chl *a* dynamics, indicating that phytoplankton production is the primary driver of particulate organic matter (POM) accumulation. Despite a shift in environmental N:P from 16 to 1000 due to nitrogen enrichment, POC:PON and PON:POP ratios remained unchanged on days 15 and 23, suggesting that phytoplankton possess a robust capacity to maintain internal elemental stoichiometry despite large fluctuations in external nutrient ratios. A previous study showed that planktonic C:P and N:P ratios rose markedly in the late twentieth century, followed by a decline, which is likely to be driven by P inputs (Liu et al. 2025). The present study indicate that short-term variations of nutrient perturbations may not change planktonic elemental stoichiometry.

On the other hand, POC:PON decreased and PON:POP increased under HN conditions on day 31, although N:P in seawater decreased from the peak of 570.73 to 22.63. This finding indicates that the effects of seawater N:P variation on phytoplankton N:P were hysteretic. Environmental restoration in N:P cannot restore phytoplankton N:P immediately. Furthermore, HN-F led to high ratios of C:P and N:P. The combination of ocean acidification and warming can enhance carbon fixation of phytoplankton (Gao et al. 2017), thus increasing POC and its ratio to POP. Ocean acidification and warming can also enhance algal nitrogen assimilation (Hoppe et al. 2018, Xu et al. 2017), thus elevating PON and its ratio to POP. The findings in the present study indicate that future ocean may lead to large deviation from Redfield ratios. Increased POC:POP and PON:POP along with decreased POC:PON in phytoplankton can propagate through food webs, affecting higher trophic levels such as fish, with potential implications for fisheries production and nutritional quality.

5. Conclusion

This study integrated biochemical analyses, plankton community profiling, and ecological stability assessments to investigate the response of phytoplankton communities to nitrogen restructuring, aiming to identify strategies for mitigating marine phytoplankton ecosystem collapse. Key findings reveal that phytoplankton communities under the present scenario (HN-P) exhibit superior resistance and recovery capacity compared to those under the future scenario (HN-F) when subjected to N:P enrichment and subsequent restoration. This highlights the urgency of implementing N:P restoration measures to prevent ecosystem degradation. Moreover, N:P perturbations, in combination with Si deficiency and climate drivers (warming and acidification), reshaped phytoplankton community structure, triggering a shift from diatom dominance to chlorophyte dominance alongside increased dinoflagellate abundance. Such shifts may increase the risk of harmful algal blooms, particularly due to the expansion of dinoflagellate populations in future scenarios. Our research provides novel insights into the ecological management and protection of subtropical coastal ecosystems, emphasizing the need for targeted nitrogen restructuring in coastal marine areas. Special consideration should be given to regions with limited water exchange, where excessive nitrogen loading may compromise the effectiveness of restoration strategies. Overall, these findings underscore the importance of integrating nutrient regulation with climate change mitigation to safeguard coastal ecosystem stability. Notably, this 32-day experiment may not fully capture the long-term impacts of climate change. Future mesocosm studies with extended incubation periods are therefore recommended to further explore phytoplankton-grazer dynamics and the adaptive capacity of plankton to ongoing climate change. In addition, future studies should include additional treatments to disentangle the individual effects of N:P ratios, Si availability, warming, and acidification on plankton community dynamics.

CRediT authorship contribution statement

Jichen Chen: Writing – review & editing, Writing – original draft, Investigation, Data curation. **Yonglong Xiong:** Investigation. **Jingke Ge:** Investigation. **Xin Zhao:** Investigation. **Yuan Feng:** Investigation. **Xu Li:** Investigation. **Chi Song:** Investigation. **Xiao Yang:** Investigation. **Rui Zhang:** Investigation. **Jin-Yu Terence Yang:** Methodology, Investigation. **Wuchang Zhang:** Methodology, Investigation. **Shengyao Sun:** Resources. **Chao Zhang:** Methodology. **Huijie Xue:** Writing – review & editing, Methodology. **Dazhi Wang:** Visualization, Validation, Supervision, Funding acquisition. **Kunshan Gao:** Resources. **Guang Gao:** Writing – review & editing, Visualization, Validation, Supervision, Funding acquisition, Formal analysis, Conceptualization.

Declaration of competing interest

The authors declare that they have no known competing financial interests or personal relationships that could have appeared to influence the work reported in this paper.

Acknowledgements

This work was supported by the National Key Research and Development Program of China (2022YFC3105304), the Open Project of Key Laboratory of Marine Environmental Survey Technology and Application, Ministry of Natural Resources (MESTA-2024-A001), the International Cooperation Seed Funding Project for China's Ocean Decade Actions (GHZZ3702840002024020000020), the Fujian Provincial Science and Technology Planning Projects (2022L3001), the Fujian Special Fund for the Development of Marine and Fishery (FJHYF-ZH-2023-04).

The authors were grateful to the laboratory technicians Wenyan Zhao, Xianglan Zeng and Yutong Yang, the students of Zheng Chen, Hongwei Wang, Lunbi Wu and Menghao Ma for their contribution to the implementation of the mesocosm experiments. Additionally, the authors acknowledge the PhD Fellowship provided by the State Key Laboratory of Marine Environmental Science, Xiamen University.

Supplementary materials

Supplementary material associated with this article can be found, in the online version, at doi:10.1016/j.watres.2026.125438.

Data availability

Data will be made available on request.

References

Andersen, I.M., Williamson, T.J., González, M.J., Vanni, M.J., 2019. Nitrate, ammonium, and phosphorus drive seasonal nutrient limitation of chlorophytes, cyanobacteria, and diatoms in a hyper-eutrophic reservoir. Limnol. Ocean 65 (5), 962–978.
Atwood, K., Knoll, L.B., 2025. Phytoplankton nutrient limitation persists into the winter in a productive midwestern US reservoir. Inland. Waters. 1–41.
Benedetti, F., Vogt, M., Elizondo, U.H., Righetti, D., Zimmermann, N.E., Gruber, N., 2021. Major restructuring of marine plankton assemblages under global warming. Nat. Commun. 12 (1), 1–15.
Chavez, F.P., Messié, M., Pennington, J.T., 2011. Marine primary production in relation to climate variability and change. Ann. Rev. Mar. Sci. 3 (1), 227–260.
Cowlishaw, R.J., 2002. The impact of differential grazing by phagotrophic ciliates on phytoplankton biomass and community structure. J. Phycol. 36 (s3), 16.
Dai, M., Zhao, Y., Chai, F., Chen, M., Chen, N., Chen, Y., Cheng, D., Gan, J., Guan, D., Hong, Y., Huang, J., Lee, Y., Leung, K.M.Y., Lim, P.E., Lin, S., Lin, X., Liu, X., Liu, Z., Luo, Y.-W., Meng, F., Sangmanee, C., Shen, Y., Uthaipan, K., Wan Talaat, W.I.A., Wan, X.S., Wang, C., Wang, D., Wang, G., Wang, S., Wang, Y., Wang, Y., Wang, Z., Wang, Z., Xu, Y., Yang, J.-Y.T., Yang, Y., Yasuhara, M., Yu, D., Yu, J., Yu, L., Zhang, Z., Zhang, Z., 2023a. Persistent eutrophication and hypoxia in the coastal ocean. Camb. Prisms.: Coast. Futures 1, 1–28.
Dai, Y., Yang, S., Zhao, D., Hu, C., Xu, W., Anderson, D.M., Li, Y., Song, X.-P., Boyce, D. G., Gibson, L., Zheng, C., Feng, L., 2023b. Coastal phytoplankton blooms expand and intensify in the 21st century. Nature 615 (7951), 280–284.
Damar, A., Prismayanti, A.D., Rudianto, B.Y., Ramli, A., Kurniawan, F., 2021. Algae bloom phenomenon in Jakarta Bay as symptoms of severe eutrophication: Monitoring results of 2014-2016. Int. Symp. Aquat. Sci. Resour. Manag. 744, 1–10.
Derolez, V., Bec, B., Munaron, D., Fiandrino, A., Pete, R., Simier, M., Souchu, P., Laugier, T., Aliaume, C., Malet, N., 2019. Recovery trajectories following the reduction of urban nutrient inputs along the eutrophication gradient in French Mediterranean lagoons. Ocean Coast. Manag. 171, 1–10.
Duarte, C.M., Conley, D.J., Carstensen, J., Sánchez-Camacho, M., 2008. Return to neverland: Shifting baselines affect eutrophication restoration targets. Estuaries Coasts. 32 (1), 29–36.
Feng, Y., Xiong, Y., Hall-Spencer, J.M., Liu, K., Beardall, J., Gao, K., Ge, J., Xu, J., Gao, G., 2023. Shift in algal blooms from micro- to macroalgae around China with increasing eutrophication and climate change. Glob. Chang. Biol. 30 (1), 1–16.
Gao, G., Jin, P., Liu, N., Li, F., Tong, S., Hutchins, D.A., Gao, K., 2017. The acclimation process of phytoplankton biomass, carbon fixation and respiration to the combined effects of elevated temperature and pCO_2 in the northern South China Sea. Mar. Pollut. Bull. 118 (1–2), 213–220.
Gao, G., Zhao, X., Jiang, M., Gao, L., 2021. Impacts of marine heatwaves on algal structure and carbon sequestration in conjunction with ocean warming and acidification. Front. Mar. Sci. 8, 758651.
Gao, K., Gao, G., Wang, Y., Dupont, S., 2020. Impacts of ocean acidification under multiple stressors on typical organisms and ecological processes. Mar. Life Sci. Technol. 2 (3), 279–291.
Hillebrand, H., Langenheder, S., Lebret, K., Lindström, E., Östman, Ö., Striebel, M., O'Connor, M., 2017. Decomposing multiple dimensions of stability in global change experiments. Ecol. Lett. 21 (1), 21–30.
Hoppe, C.J.M., Flintrop, C.M., Rost, B., 2018. The Arctic picoeukaryote Micromonas pusilla benefits synergistically from warming and ocean acidification. Biogeosciences. 15 (14), 4353–4365.
Huang, R., Sun, J., Yang, Y., Jiang, X., Wang, Z., Song, X., Wang, T., Zhang, D., Li, H., Yi, X., Chen, S., Bao, N., Qu, L., Zhang, R., Jiao, N., Gao, Y., Huang, B., Lin, X., Gao, G., Gao, K., 2021. Elevated pCO_2 impedes succession of phytoplankton community from diatoms to dinoflagellates along with increased abundance of viruses and bacteria. Front. Mar. Sci. 8, 642208.
IPCC, 2023. IPCC, 2023: Summary for policymakers. Climate change 2023: Synthesis report. Contribution of Working Groups I, II and III to the Sixth Assessment Report of the Intergovernmental Panel on Climate Change, pp. 1–34.
Ives, A.R., Carpenter, S.R., 2007. Stability and diversity of ecosystems. Science 1979 317, 58–62.
Jeppesen, E., Søndergaard, M., Meerhoff, M., Lauridsen, T.L., Jensen, J.P., 2007. Shallow lake restoration by nutrient loading reduction—some recent findings and challenges ahead. Hydrobiologia 584 (1), 239–252.
Jiang, D., Zhang, H., 2018. Analysis of spatial and temporal characteristics of chlorophyll-a concentration and red tide monitoring in Bohai Sea (in Chinese version). Mar. Sci. 42 (5), 23–31.
Landry, M.R., Hassett, R.P., 1982. Estimating the grazing impact of marine micro-zooplankton. Mar. Biol. 67, 283–288.
Liu, J., Wang, H., Mou, J., Penuelas, J., Delgado-Baquerizo, M., Martiny, A.C., Zhou, G., Hutchins, D.A., Inomura, K., Lomas, M.W., Fakhraee, M., Pellegrini, A., Kohler, T.J., Deutsch, C.A., Planavsky, N., Lapointe, B., Zhang, Y., Li, Y., Zhou, J., Zhang, Y., Sun, S., Li, Y., Zhang, W., Cao, J., Chen, J., 2025. Global-scale shifts in marine ecological stoichiometry over the past 50 years. Nat. Geosci. 18 (8), 769–778.
McCann, K.S., 2000. The diversity–stability debate. Nature 405, 228–233.
McCrackin, M.L., Jones, H.P., Jones, P.C., Moreno-Mateos, D., 2016. Recovery of lakes and coastal marine ecosystems from eutrophication: A global meta-analysis. Limnol. Ocean 62 (2), 507–518.
MorÁN, X.A.G., LÓPez-Urrutia, Á., Calvo-DÍAz, A., Li, W.K.W, 2010. Increasing importance of small phytoplankton in a warmer ocean. Glob. Chang. Biol. 16 (3), 1137–1144.
Pešová, D., Macek, M., Elena Martínez Pérez, M., 2008. Ciliates and their picophytoplankton-feeding activity in a high-altitude warm-monomictic saline lake. Eur. J. Protistol. 44 (1), 13–25.
Pierrot, D., Wallace, D., Lewis, E., 2011. MS excel program developed for CO_2 system calculations. Carbon Dioxide Inf. Anal. Cent.
Raven, J.A., Giordano, M., Beardall, J., Maberly, S.C., 2011. Algal and aquatic plant carbon concentrating mechanisms in relation to environmental change. Photosynth. Res. 109 (1-3), 281–296.
Ritchie, R.J., 2006. Consistent sets of spectrophotometric chlorophyll equations for acetone, methanol and ethanol solvents. Photosynth. Res. 89 (1), 27–41.
Roy, R.N., Roy, L.N., Vogel, K.M., Porter-Moore, C., Pearson, T., Good, C.E., Millero, F.J., Campbell, D.M., 1993. The dissociation constants of carbonic acid in seawater at salinities 5 to 45 and temperatures 0 to 45°C. Mar. Chem. 44 (2-4), 249–267.
Ryan, J.P., Kudela, R.M., Birch, J.M., Blum, M., Bowers, H.A., Chavez, F.P., Doucette, G. J., Hayashi, K., Marin, R., Mikulski, C.M., Pennington, J.T., Scholin, C.A., Smith, G. J., Woods, A., Zhang, Y., 2017. Causality of an extreme harmful algal bloom in Monterey Bay, California, during the 2014–2016 northeast Pacific warm anomaly. Geophys. Res. Lett. 44 (11), 5571–5579.
Sidabutar, T., Bengen, D.G., Wouthuyzen, S.A.M., Partono, T.R.I., 2016. The abundance of phytoplankton and its relationship to the N/P ratio in Jakarta Bay, Indonesia. Biodiversitas. J. Biol. Divers 17 (2), 673–678.
Sieracki, M.E., Verity, P.G., Stoecker, D.K., 1993. Plankton community response to sequential silicate and nitrate depletion during the 1989 North Atlantic spring bloom. Deep Sea Res. II: Top Stud. Oceanogr. 40 (1-2), 213–225.
Solórzano, L., Sharp, J.H., 1980. Determination of total dissolved phosphorus and particulate phosphorus in natural waters. Limnol. Ocean 25 (4), 754–758.
Soulié, T., Vidussi, F., Mas, S., Mostajir, B., 2022. Functional stability of a coastal mediterranean plankton community during an experimental marine heatwave. Front. Mar. Sci. 9, 1–17.
Utermöhl, H., 1958. Zur vervollkommnung der quantitativen phytoplankton-methodik (Towards the improvement of quantitative phytoplankton methodology). Mitteilungen Internationale Vereinigung Theoretische Angewandte Limnologie, 9, pp. 1–38.
Wang, J., Bouwman, A.F., Liu, X., Beusen, A.H.W., Van Dingenen, R., Dentener, F., Yao, Y., Glibert, P.M., Ran, X., Yao, Q., Xu, B., Yu, R., Middelburg, J.J., Yu, Z., 2021. Harmful algal blooms in Chinese coastal waters will persist due to perturbed nutrient ratios. Env. Sci. Technol. Lett. 8 (3), 276–284.
Wei, Y., Luan, Q., Shan, X., Cui, H., Qu, K., Cui, Z., Sun, J., 2024. Temperature and nutrients drive distinct successions between diatoms and dinoflagellates over the past 40 years: Implications for climate warming and eutrophication. Sci. Total. Environ. 931, 172997.
Xiao, W., Liu, X., Irwin, A.J., Laws, E.A., Wang, L., Chen, B., Zeng, Y., Huang, B., 2018. Warming and eutrophication combine to restructure diatoms and dinoflagellates. Water. Res. 128, 206–216.
Xu, Z., Gao, G., Xu, J., Wu, H., 2017. Physiological response of a golden tide alga (*Sargassum muticum*) to the interaction of ocean acidification and phosphorus enrichment. Biogeosciences. 14 (3), 671–681.
Xue, C., 2024. Automatic identification technology of plankton based on image generation (Chinese version). Xiamen University, Xiamen, China. Master's thesis.
Zadereev, E., Lopatina, T., Ovchinnikov, S., Tolomeev, A., 2023. Grazing rate and feeding selectivity of small and large bodied cladocerans in waters from lakes with different salinity and phytoplankton structure. J. Ocean Limnol. 41 (4), 1341–1351.